Bifurcation analysis of solitary and synchronized pulses and formation of reentrant waves in laterally coupled excitable fibers

Tatsuo Yanagita*
Research Institute for Electronic Science, Hokkaido University, Sapporo 001-0020, Japan

Hiromichi Suetani
Department of Physics, Kagoshima University, Kagoshima 890-0065, Japan
and Decoding and Controlling Brain Information, PRESTO, JST, Kawaguchi 332–0012, Japan

Kazuyuki Aihara
Institute of Industrial Science, The University of Tokyo, Tokyo 153-8505, Japan
and Aihara Complexity Modelling Project, ERATO, JST, Tokyo 153–8505, Japan
(Received 18 April 2008; published 13 November 2008)

We study the dynamics of a reaction-diffusion system comprising two mutually coupled excitable fibers. We consider a case in which the dynamical properties of the two fibers are nonidentical due to the parameter mismatch between them. By using the spatially one-dimensional FitzHugh-Nagumo equations as a model of a single excitable fiber, synchronized pulses are found to be stable in some parameter regime. Furthermore, there exists a critical coupling strength beyond which the synchronized pulses are stable for any amount of parameter mismatch. We show the bifurcation structures of the synchronized and solitary pulses and identify a codimension-2 cusp singularity as the source of the destabilization of synchronized pulses. When stable solitary pulses in both fibers disappear via a saddle-node bifurcation on increasing the coupling strength, a reentrant wave is formed. The parameter region, where a stable reentrant wave is observed in direct numerical simulation, is consistent with that obtained by bifurcation analysis.

DOI: 10.1103/PhysRevE.78.056208 PACS number(s): 05.45.−a, 82.40.Bj

I. INTRODUCTION

Synchronization is a ubiquitous dynamical property encountered in many fields of science, and it plays an important role in the functional aspects of many living systems [1]. Most pioneering studies on these living systems have focused on the synchronization between rhythmic phenomena [2]. Recently, synchronization via interaction between spatiotemporal patterns has attracted considerable interest. Then, it is well known that excitability plays an important role in various systems in nature, such as heart tissues [3–6], neurons [7–9], aggregating amoebae [10,11], the catalytic CO oxidation reactions on a Pt surface [12–15], chemical reactions [16,17], and lasers [18–20]. In this study, we investigate the bifurcation structure of pulse solutions emanating from the interaction between spatiotemporal patterns, i.e., propagating pulses in coupled excitable media.

In the case of simple excitable elements, a small but finite perturbation to the rest state leads to a large excursion (an excitation). When a system is spatially extended, it is known that a localized stimulus of a finite amplitude forms stable propagating pulses. These large pulses or excited spikes have a proper shape, which is usually dictated by a low-dimensional phase space. In systems such as a bundle of nerve fibers or heart tissues, the large pulses are associated with an action potential (AP).

Spatially extended excitable media are usually modeled within the framework of reaction-diffusion systems, and they show a rich variety of dynamical behaviors, including propagating pulses and target waves [21], spiral waves [22], and spatiotemporal chaos [23]. Recently, reaction-diffusion systems in excitable media and the interaction between these systems have attracted considerable interest, as stated above. For example, in [24], it has been reported that the mutual interaction between the stationary Turing patterns existing in one layer and the oscillatory waves existing in another layer, which is brought about by the layer-coupling method, yields a large variety of oscillatory Turing patterns. Complete synchronization of spiral waves was experimentally demonstrated for two mutually coupled Belouzov-Zhabotinsky chemical reaction media [25]. Later, the time-lag synchronization of spatiotemporal disorders was also observed in a pair of unidirectionally coupled nonlinear optical systems [26]. From the engineering viewpoint, spatially synchronized chaos in optical systems has potential applications in communication [27].

Furthermore, mutually coupled excitable media are extensively used as models of heart tissues and bundles of nerve fibers. A short review of these models is given below.

As a bundle of nerve fibers. Most neurons have complicated shapes; the bifurcation patterns in dendrites and axon terminals are particularly complex. Further, dendrites tend to bifurcate repeatedly and create a (often several) large and complicated tree. A particular dendritic morphology behaves like a complex dynamical device with potentially rich repertories of input-output capabilities [28–32]. The above examples suggest that pulse-pulse interactions might play a crucial role in determining the dynamical behavior and information processing in a neuronal system. However, these

*yanagita@nsc.es.hokudai.ac.jp; http://www-nsc.es.hokudai.ac.jp/~yanagita

pulse-pulse interactions exist not only in specific spatial regions but also along myelinated nerve fibers that are parallel and relatively close together through mutually propagated pulses. Such parallel fiber interactions have been known to electrophysiologists since the 1940s [33,34] and are termed ephaptic, derived from a Greek word meaning "to touch" [35].

As a model of heart tissues. Laterally coupled excitable media can be used to study cardiac tachycardias, which are abnormal cardiac rhythms in which the heartbeat is very rapid [36,37]. The interaction between pulses propagating in a fiber is important in a cardiac system; this interaction induces instabilities and entrainment of pulse propagation [4,5,38,39]. However, the real heart with its several different structures and inhomogeneities is an inhomogeneous system. Heart cells are cylindrical and are structurally arranged in parallel arrays in local regions, although the axis of fiber orientation varies from one region of the heart to the other [40]. For example, the Purkinje fibers form a network structure. The excitation pulse propagates several times faster in the Purkinje fibers than in the normal ventricular tissues. The assumption that a cardiac tissue is a two-phase medium consisting of intracellular and extracellular spaces leads to laterally coupled excitable equations called the bidomain model [41,42]. A pair of continuous one-dimensional fibers coupled electrotonically in the lateral direction is used as a simple example of a two-dimensional medium [43].

In laterally coupled excitable fibers, synchronization between two pulses, each propagating along an identical fiber, and repeated excitation in a specific region, called the reentrant wave, have been observed. Such pattern dynamics are related to many biological problems. For example, the reentrant wave is considered to be the cause of heart condition such as tachycardias and fibrillation [44,45]. Further, laterally coupled fibers can also be used to study the ephaptic (nonsynaptic) interactions between the impulses in parallel fibers since the myelinated nerve fibers are often arranged in bundles [46,47]. The conduction velocities in neighboring fibers might be combined due to the ephaptic interaction between adjacent axons, thereby causing the synchronizing activity in a bundle of axons, which may play a functional role in neural processing [48,49].

It is also shown that various types of pulse dynamics such as solitonlike collisions between two pulses, recombination of synchronized pulses, and phase locking between two pulses are found in the spatially one-dimensional FitzHugh-Nagumo (FHN) equations when the intradiffusion coefficients of two media are nonidentical [50]. Solitary waves are also found in excitable systems with cross diffusion [51,52].

In this paper, by using the spatially one-dimensional FHN equations as a simple model of an excitable fiber, we focus our attention on synchronized pulses and reentrant waves when parallel fibers are laterally coupled. A detailed bifurcation structure for these pattern dynamics is revealed in this paper.

II. MODEL

Spatially extended excitable media are usually modeled within the framework of reaction-diffusion systems. In this paper, we consider mutually coupled excitable fibers.

For simplicity, we assume that the dynamics of the fibers is represented by the same model equation. We consider a two-layer model of the FHN equations. The system consists of the following equations:

$$\partial_t U_1 = U_1(U_1 - \alpha)(1 - U_1) - V_1 + \kappa_1 \nabla^2 U_1 + \epsilon(U_2 - U_1),$$

$$\partial_t V_1 = \tau(U_1 - \gamma V_1),$$

$$\partial_t U_2 = U_2(U_2 - \alpha)(1 - U_2) - V_2 + \kappa_2 \nabla^2 U_2 + \epsilon(U_1 - U_2),$$

$$\partial_t V_2 = \tau(U_2 - \gamma V_2). \quad (1)$$

Subscripts 1 and 2 denote fiber 1 and fiber 2, respectively. The state variables $U_{1,2}=U_{1,2}(x,t)$ and $V_{1,2}=V_{1,2}(x,t)$ are the activators (the membrane potentials) and the inhibitors (the recovery variables), respectively; in this case, $x \in [0,L]$ and $t \in [0,\infty)$ are the space and time coordinates, respectively.

The coupling between the fibers is assumed to be electrotonic, so that the current flow between them is proportional to the potential difference across them. Thus, for the activators, the mutual interaction between two excitable fibers can be introduced as the linear coupling terms $\epsilon(U_{1,2}-U_{2,1})$. The coupling coefficient ϵ is inversely proportional to the resistance between the fibers.

One physiological setting where this model may be relevant is in the bundle of His. It has been suggested that in a bundle of parallel fibers, an AP may travel along some but not all fibers, and in this manner, a bundle of Purkinje fibers can support multiple dissociated pathways. For example, certain reciprocating rhythms may result from an impulse that travels in one direction along one fiber or a bundle of fibers and then "crosses over" to another fiber and propagates in the retrograde direction. These rhythms may be the cause of continuously circulating excitation waves that are considered to exist in the Purkinje fibers. Another possible physiological implication of this two-layer model is that one layer represents a ventricular tissue and the other layer represents the Purkinje fibers, assuming that the Purkinje fiber network covers the ventricular tissue.

The parameters of the reaction kinetics are set as $\alpha = 10^{-1}, \tau = 2 \times 10^{-3}$, and $\gamma = 2.5$, so that the local kinetics shows an excitable property, i.e., a small but finite perturbation to the resting state $(u,v)=(0,0)$ leads to a large excursion. The terms $\nabla^2 U_{1,2} = \partial^2 U_{1,2}/\partial x^2$ represent intrafiber diffusions with coefficients κ_1 and κ_2. The value of κ_1 is set to 0.25 throughout this paper.

Because the system is spatially one dimensional and has simple reaction kinetics (monostable rest state), the traveling pulse is only a nontrivial solution without any coupling between the fibers.

In numerical simulations, we use the Euler integration scheme with a time step $\Delta t = 10^{-2}$ and a spatial step $\Delta x = 5 \times 10^{-1}$. The diffusion terms at a spatial point x_i $(=i\Delta x)$ are approximated as $\nabla^2 U_{1,2}(x_i) = [1/(\Delta x)^2][U_{1,2}(x_{i-1}) - 2U_{1,2}(x_i) + U_{1,2}(x_{i+1})]$. The following periodic boundary condition is employed for both the fibers: $U_{1,2}(0,t) = U_{1,2}(L,t)$.

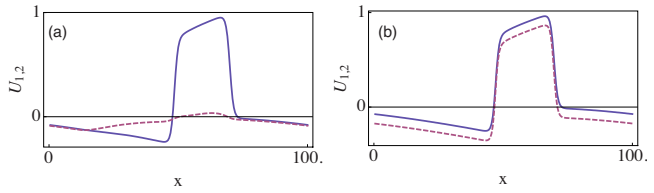

FIG. 1. (Color online) Spatial pattern of (a) solitary pulse, $\epsilon=0.001$ and (b) synchronized pulses, $\epsilon=0.1$. The solid and broken lines are the pulses in fiber 1 (U_1) and in fiber 2 (U_2), respectively. For synchronized pulses, the $U_2-0.1$ value is plotted. The parameters are $\tau=0.02$, $\alpha=0.1$, and $\kappa_1=\kappa_2=0.25$.

III. NUMERICAL SIMULATIONS OF SYNCHRONIZED PULSES AND REENTRANT WAVES

In numerical simulations, we use the following initial conditions:

$$U_1(x,0)=\begin{cases}0 & \text{for } 0\leqslant x\leqslant 0.48L,\\ 1 & \text{for } 0.48L<x<0.52L,\\ 0 & \text{for } 0.52L\leqslant x<L,\end{cases} \tag{2}$$

$$V_1(x,0)=\begin{cases}0.1 & \text{for } 0\leqslant x\leqslant 0.48L,\\ 0 & \text{for } 0.48L\leqslant x<L\end{cases} \tag{3}$$

for fiber 1, and

$$U_2(x,0)=V_2(x,0)=0 \quad \forall\, x\in[0,L] \tag{4}$$

for fiber 2. On applying these initial conditions, we can obtain a state in which a right-propagating pulse is initiated in fiber 1, while fiber 2 is set to the global resting state.

When the diffusion coefficients κ_1 and κ_2 of the two fibers are identical, we observe the following four different phases after an initial transient dies out with an increase in the interfiber coupling ϵ: (i) a solitary pulse propagating along fiber 1, (ii) formation of a reentrant wave, (iii) the global resting state after a finite repetition of reentrant waves, and (iv) synchronized pulses propagating in both the fibers. Further, when the intradiffusion coefficients of the two fibers are nonidentical, i.e., $\kappa_1\neq\kappa 2$, the following interesting pulse dynamics are observed: one-way excitation, solitonlike collision, and recombination of pulses [50].

In this paper, we analyze three basic phases: a solitary pulse, a reentrant wave, and synchronized pulses. As shown in Fig. 1(a), for a sufficiently small value of ϵ, a propagating pulse in fiber 1 cannot induce a suprathreshold excitation; however, a subthreshold excitation typically appears as a small-amplitude pulse in fiber 2. For sufficiently large values of $\epsilon>7.2\times10^{-2}$, the pulse initially generated in fiber 1 at time $t=0$ generates a new excitation in fiber 2. A right-propagating pulse emerges in fiber 2 from this excitation and immediately becomes synchronized with the pulse initially generated in fiber 1 [Fig. 1(b)]. For intermediate values of ϵ, reexcitation is observed in the following manner (Fig. 2 shows a series of spatial profiles with $\epsilon=0.007$). The new excitation in fiber 2 splits into two pulses, one moving leftward and the other rightward ($t=100$). The right-propagating pulse in fiber 2 immediately becomes synchronized with that

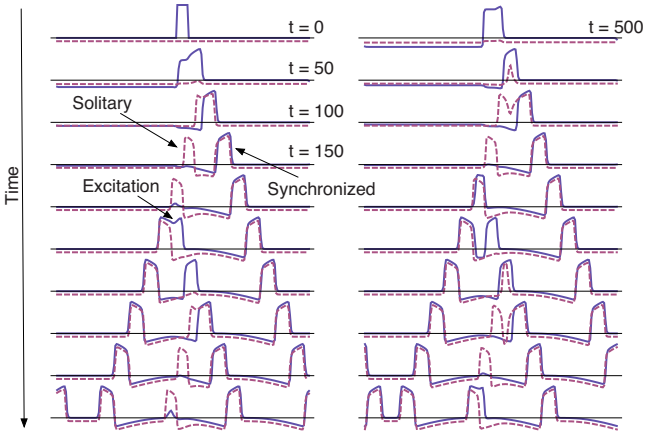

FIG. 2. (Color online) Successive images of the spatial profiles of U_1 and $U_2-0.1$ of the reentrant wave. The solid and broken lines represent U_1 and $U_2-0.1$, respectively. For the waves in fiber 2, $U_2-0.1$ is plotted. The value of ϵ is 0.007, and the other parameters are the same as those in Fig. 1.

in fiber 1 ($t=150$), whereas the left-propagating pulse in fiber 2 remains solitary. Because of a refractory region behind the right-propagating pulse in fiber 1, this solitary pulse requires some time to induce the next excitation in fiber 1 ($t=250$). Then, two pulses propagating in opposite directions emerge from the excitation induced in fiber 1; due to the solitary pulse, the left-propagating pulse in fiber 1 is synchronized with the previously generated pulse in fiber 2, while the right-propagating pulse in fiber 1 remains solitary for some time. This right-propagating pulse again will be able to cause an excitation in fiber 2 in the course of time. These processes occur repetitively in a specific region. The dynamical pattern associated with such repetition is called the reentrant wave [53–56]. The spatiotemporal patterns of the three phases—solitary pulse, reentrant wave, and synchronized pulses—are shown in Fig. 3.

IV. BIFURCATION ANALYSIS

For full partial differential equations (PDEs) (1), we study the stationary solutions in which the pulses propagate with a constant velocity c. On transforming to a comoving frame $\xi=x-ct$, Eq. (1) becomes

$$\begin{aligned}\partial_t u_1 &= u_1(u_1-\alpha)(1-u_1)+c\partial_\xi u_1+\kappa_1\partial_{\xi\xi}u_1+\epsilon(u_2-u_1),\\ \partial_t v_1 &= \tau(u_1-\gamma v_1),\\ \partial_t u_2 &= u_2(u_2-\alpha)(1-u_2)+c\partial_\xi u_2+\kappa_2\partial_{\xi\xi}u_2+\epsilon(u_1-u_2),\\ \partial_t v_2 &= \tau(u_2-\gamma v_2).\end{aligned} \tag{5}$$

A stationary solution propagating with a velocity c corresponds to the condition $\partial_t u_i=\partial_t v_i=0$. In this case, the problem can be reduced to a traveling wave ordinary differential equation (ODE) for the spatial profile in the following form:

$$\frac{du_1}{d\xi}=w_1,$$

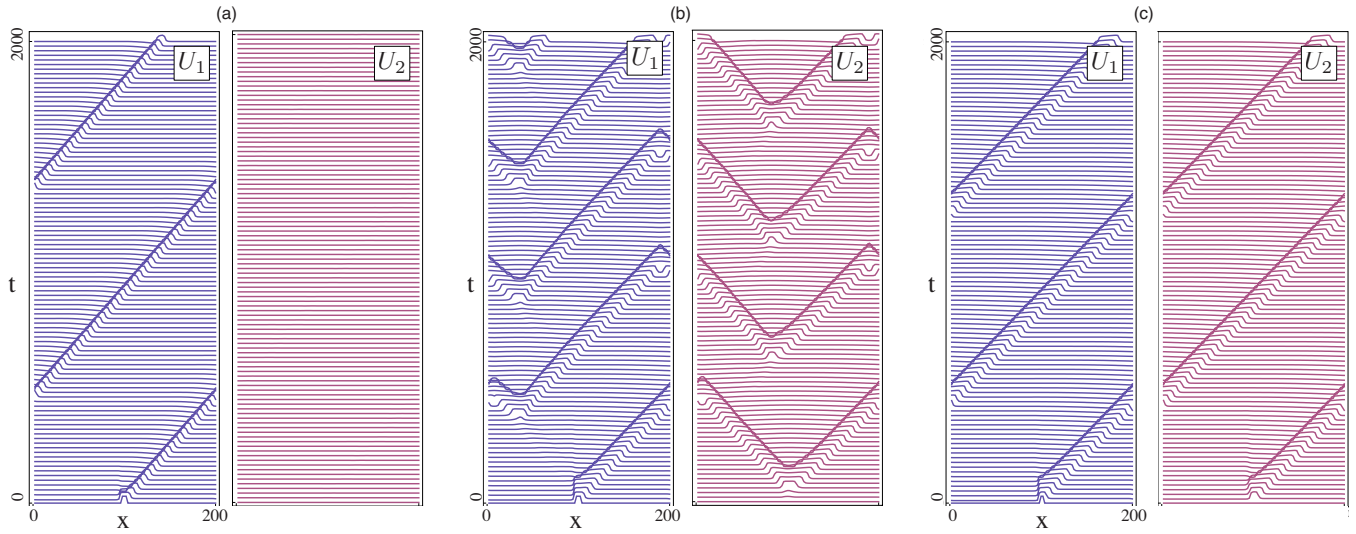

FIG. 3. (Color online) Spatiotemporal patterns for U_1 (left) and U_2 (right). (a) Solitary pulse: $\epsilon=0.001$, (b) reentrant waves, $\epsilon=0.009$, and (c) synchronized pulses, $\epsilon=0.08$. The other parameters are the same as those in Fig. 1.

$$\frac{dw_1}{d\xi} = \frac{-cw_1 - u_1(u_1-\alpha)(1-u_1) - \epsilon(u_2-u_1)}{\kappa_1},$$

$$\frac{dv_1}{d\xi} = -\frac{\tau}{c}(u_1 - \gamma v_1),$$

$$\frac{du_2}{d\xi} = w_2,$$

$$\frac{dw_2}{d\xi} = \frac{-cw_2 - u_2(u_2-\alpha)(1-u_2) - \epsilon(u_1-u_2)}{\kappa_2},$$

$$\frac{dv_2}{d\xi} = -\frac{\tau}{c}(u_2 - \gamma v_2). \tag{6}$$

We immediately see that if $(u_i,v_i)=(0,0)$ is a fixed point of the kinetics, then $(u_i,w_i,v_i)=(0,0,0)$ is also a fixed point in Eq. (6).

Solutions of traveling wave ODEs such as fixed points, periodic orbits, and homoclinic and heteroclinic connections, correspond to homogeneous solutions, traveling waves, pulses in a homogeneous state, and fronts connecting two different homogeneous solutions, respectively, for the PDE (see [57] for a general review). The above considerations allow us to study the properties of nonlinear waves by using well-established dynamical systems methods such as bifurcation analysis and the continuation of a solution in parameter space [58]. In this approach, a solitary excited pulse, which travels on a spatially homogeneous background $(U_i,V_i)=(0,0)$, corresponds to a homoclinic orbit to the equilibrium point $(u_i,w_i,v_i)=(0,0,0)$ in Eq. (6). A solution of a periodic wave train in the reaction-diffusion equations (1) is presented by a limit cycle in the traveling wave ODEs. Both types of solutions can be successfully tracked with the continuation software AUTO [59] along the parameters of the local reaction kinetics, the velocity c, and the wavelength L.

In the following sections, we consider a traveling wave, which is given by a periodic orbit with period $T=300$ and a certain velocity parameter c in Eq. (6) (the bifurcation structure does not significantly depend on the period T for $T>150$).

A. Solitary pulse

First, we consider the propagation of a solitary pulse on a ring. The dependence of the propagation speed c on the period T (the period of the periodic orbit of Eq. (6) corresponds to the length of the ring in Eq. (1)) is called the dispersion curve. Figure 4(a) shows the dispersion curve of a solitary pulse. The wave speed asymptotically approaches its maximum for a sufficiently large wavelength. The speed of the pulse gradually decreases with a decrease in the wavelength, and there is a finite minimum wavelength. A saddle-node (SN) bifurcation occurs at the end point, where the stable and unstable solution branches meet. The profiles of these stable and unstable pulses are shown in Fig. 4(b). The amplitude and propagation speed of the unstable solution are smaller and slower than those of the stable one, respectively.

Next, we consider the dependence of the pulse velocity on ϵ by performing the continuation of the corresponding periodic solution of equation (6). In numerical simulations, the reaction-diffusion equation (1) support the propagation of the solitary excitation pulses in the parameter region $0.0<\epsilon<7.2058\times10^{-3}$. In Fig. 5(a), the bifurcation diagram of a solitary pulse is plotted. The lower branch corresponds to a stable solitary pulse in fiber 1. When the coupling strength ϵ increases, the maximum of U_2 gradually increases along the branch by increasing the subthreshold excitation in fiber 2. The typical spatial profile of a solitary pulse in fiber 1 indicated by (i) is illustrated in Fig. 5(c). As ϵ is further increased, the stable solitary pulse disappears through a SN bifurcation at the critical value ϵ_{SN2}, and the solution branch turns back slightly in the negative direction of ϵ. The solution branch $\max_\xi u_2(\xi)$ increases suddenly near ϵ_{SN2}, where a

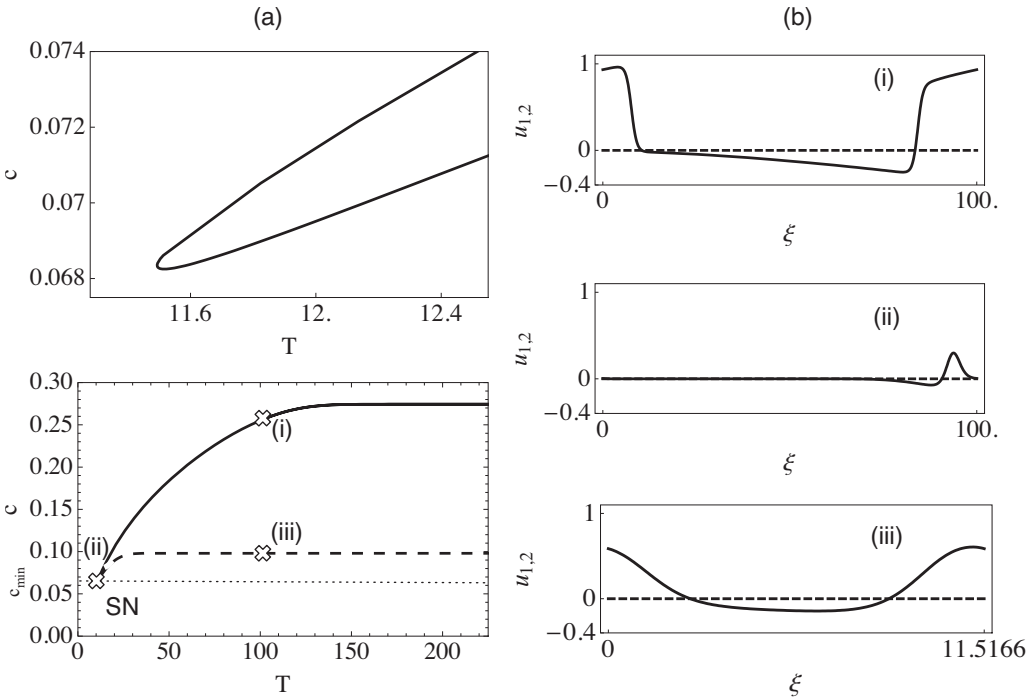

FIG. 4. (a) Dispersion curve of the solitary pulse train in fiber 1. SN denotes the saddle-node bifurcation. The upper figure shows the magnification in the vicinity of the turning point. The upper branch (the solid line) and the lower branch (the dotted line) correspond to the stable and unstable traveling wave solutions, respectively. The SN threshold is given by $T=11.5166$. (b) The corresponding solutions on the branch [indicated by the open crosses in (a)] are shown. The periodic solution: (i) the stable solution at $T=100$, (ii) the solution at the SN point, and (iii) the unstable periodic solution at $T=100$. The solid line represents $u_1(\xi)$, while the broken line represents $u_2(\xi)$.

new suprathreshold excitation emerges behind the original pulse in fiber 1. This emergence is related to canards, that is, a steep increase in the amplitude of oscillation in relaxation systems [9]. However, in this case, the bifurcation is not the Hopf type, but the SN type [9], and the amplitude of excitation does not oscillate. A sequence of images of this bifurcation process along the branch is shown in Fig. 5(c). It can be clearly observed that the amplitude of the new pulse in fiber 2 increases rapidly and the new suprathreshold excitation

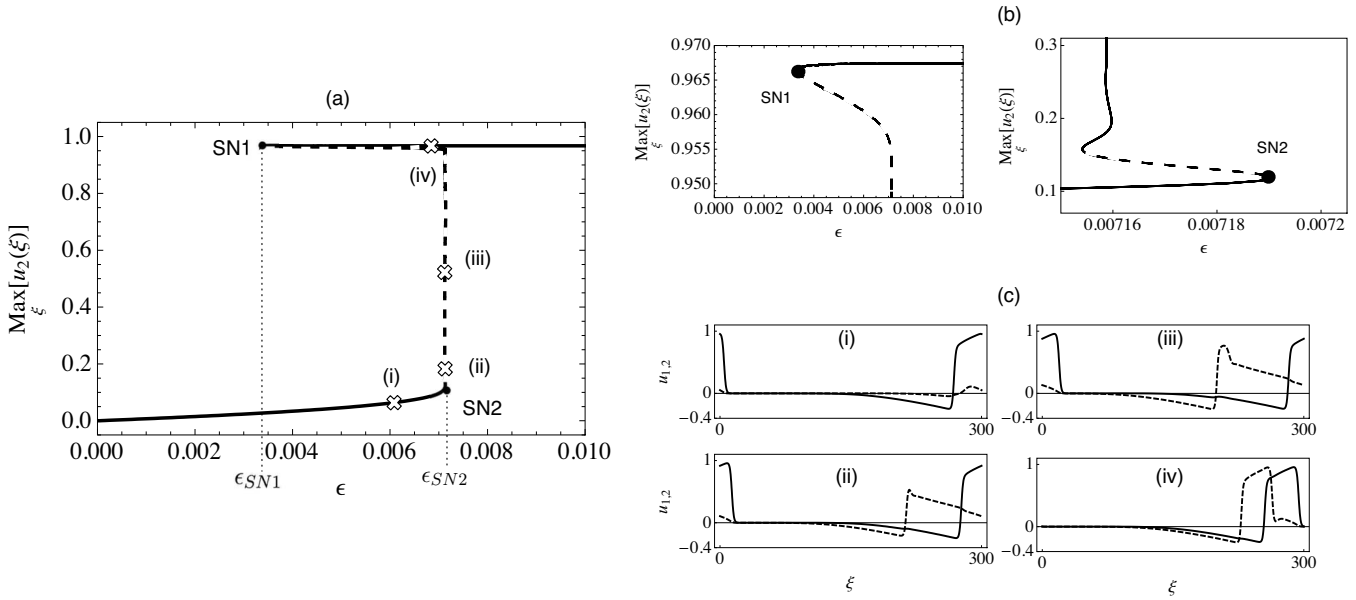

FIG. 5. (a) Bifurcation diagram of the solitary pulse in fiber 1. SN denotes the saddle-node bifurcation. The solid and broken lines correspond to stable and unstable solutions, respectively. The SN1 (SN2) threshold is given by $\epsilon_{SN1} \simeq 0.003\ 342\ 64$ ($\epsilon_{SN2} \simeq 0.007\ 130\ 27$) for $\kappa_2=0.24$. (b) Magnifications of small regions near SN1 and SN2. (c) Spatial profiles at each of the locations indicated by open crosses in (a). The emergence of a new excitation in fiber 2 near the SN2 point is clearly shown.

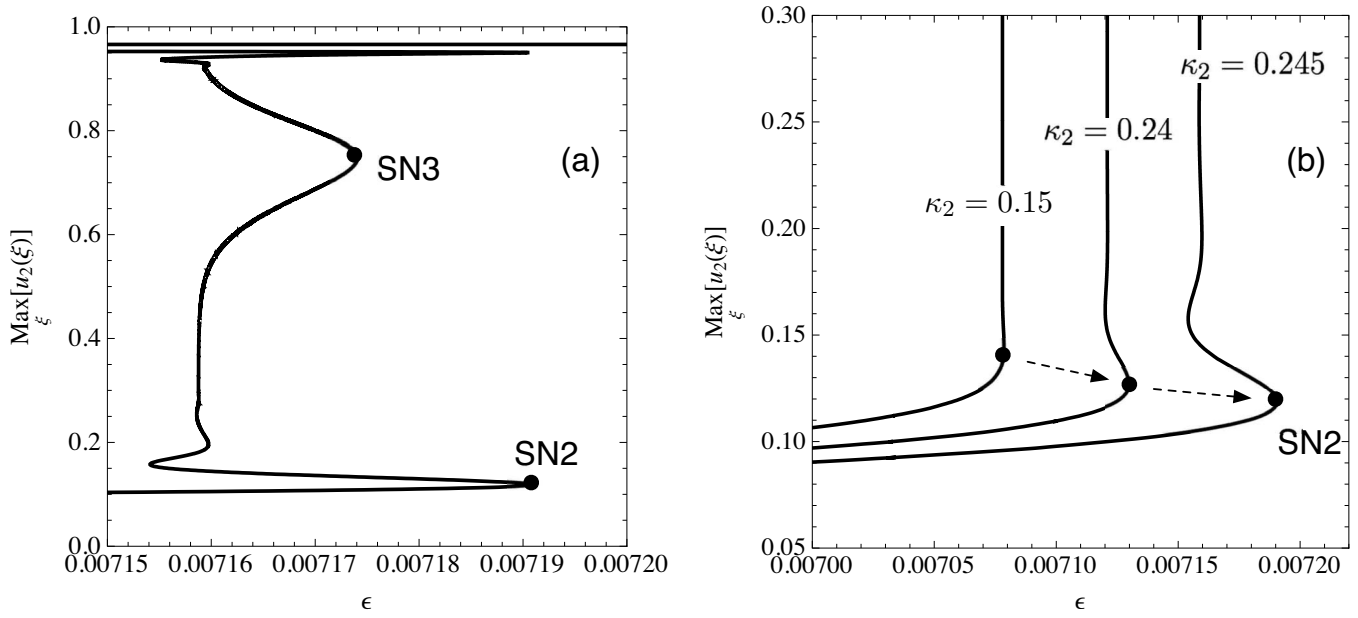

FIG. 6. (a) A magnified view of the bifurcation diagram in Fig. 5. There exist several turnback points where SN bifurcations occur. The bulge structure grows as κ_2 approaches $\kappa_1=0.25$. (b) The bulges near SN2 are plotted for $\kappa_2=0.15$, 0.24, and 0.245. The emergence and development of the bulge structure are clearly shown.

appears to form an unstable phase-locked solution [see (iii) and (iv) in Fig. 5(c)].

After the increase, the solution branch suddenly turns back in the negative direction of ϵ and another SN bifurcation occurs at ϵ_{SN1}, the meeting point of the unstable phase-locked pulses and the stable synchronized pulses. At this point, the branch again turns back in the positive direction of ϵ. The upper branch [the upper solid line in Fig. 5(a)] corresponds to stable synchronized pulses. Synchronized pulses exist above ϵ_{SN1}, but there is a time delay between the pulses. For a given value in $\epsilon_{\mathrm{SN1}} \simeq 0.003\,342\,64 < \epsilon < \epsilon_{\mathrm{SN2}} \simeq 0.007\,130\,27$, there simultaneously exist two stable stationary solutions, one solitary and one synchronized. The region in which the two solutions coexist expands as κ_2 approaches to $\kappa_1=0.25$.

Figure 6(a) shows a magnified view of Fig. 5(a) near the region in which solitary and synchronized pulses coexist (emergence of new excitation in fiber 2). The bifurcation diagram clearly shows that there are several turnback points where SN bifurcations occur. It is known that complex SN bifurcation structures exist in coupled excitable elements (ODEs) [60,61]. In Fig. 6(b), the development of the bulge at SN2 is plotted for $\kappa_2=0.15$, 0.24, and 0.245. These bulges grow as κ_2 approaches $\kappa_1=0.25$, and the region in which solitary and synchronized pulses coexist expands. As κ_2 decreases, the bulge shrinks and disappears with the merging of the SN points. However, one of the SN points, indicated by SN3 in Fig. 6(a), exists for $0 < \kappa_2 \leqslant 0.25$.

We investigate the bifurcation structure of a solitary pulse propagating in fiber 2. Because the intradiffusion coefficients are nonidentical, the bifurcation structure is different from that of a solitary pulse in fiber 1. A solitary pulse propagating in fiber 2 is stable for smaller interfiber coupling. As shown in Fig. 7(a), the solution disappears via a SN bifurcation at the critical coupling strength $\epsilon_{\mathrm{SN4}} \simeq 0.008\,116\,09$. After this SN point, the solution branch turns back slightly and successive SN bifurcations follow. Here, we use the L^2 norm, which is defined as

$$\sqrt{\int_0^T \sum_{i=1}^{2} u_i^2(\xi) + v_i^2(\xi) + w_i^2(\xi) d\xi};$$

a sudden increase in the L^2 norm is observed along the branch after several turning points. This sudden increase indicates the emergence of a new suprathreshold excitation. In the inset of Fig. 7(a), a sequence of spatial patterns along the solution branch is shown.

In the case of a solitary pulse in fiber 1, when we increase ϵ, the original pulse and a new excitation in fiber 2 form stable synchronized pulses, as shown in Fig. 5. However, in the case of a solitary pulse in fiber 2, the original solitary pulse in fiber 2 and a new excitation in fiber 1 do not form stable synchronized pulses. Instead, the successive generation of supraexcitation behind the original solitary pulse in fiber 2 is observed though a cascade of SN bifurcations. A sequence of images of the new excitation is shown in the insets of Fig. 7(a). As shown in the next subsection, the SN4 bifurcation point is related to the emergence of a reentrant wave.

B. Synchronized pulses

In this section, we investigate the bifurcation of synchronized pulses. In numerical simulations, when the difference between the intradiffusion coefficients $\Delta\kappa=\kappa_1-\kappa_2$ is small, we find that the synchronized pulses can be in the stable state for any ϵ if a pair of synchronized pulses is initiated as the initial condition [50]. Further, we observe that, beyond the critical value of $\Delta\kappa$, the synchronized pulses become unstable and split into two solitary pulses with different propa-

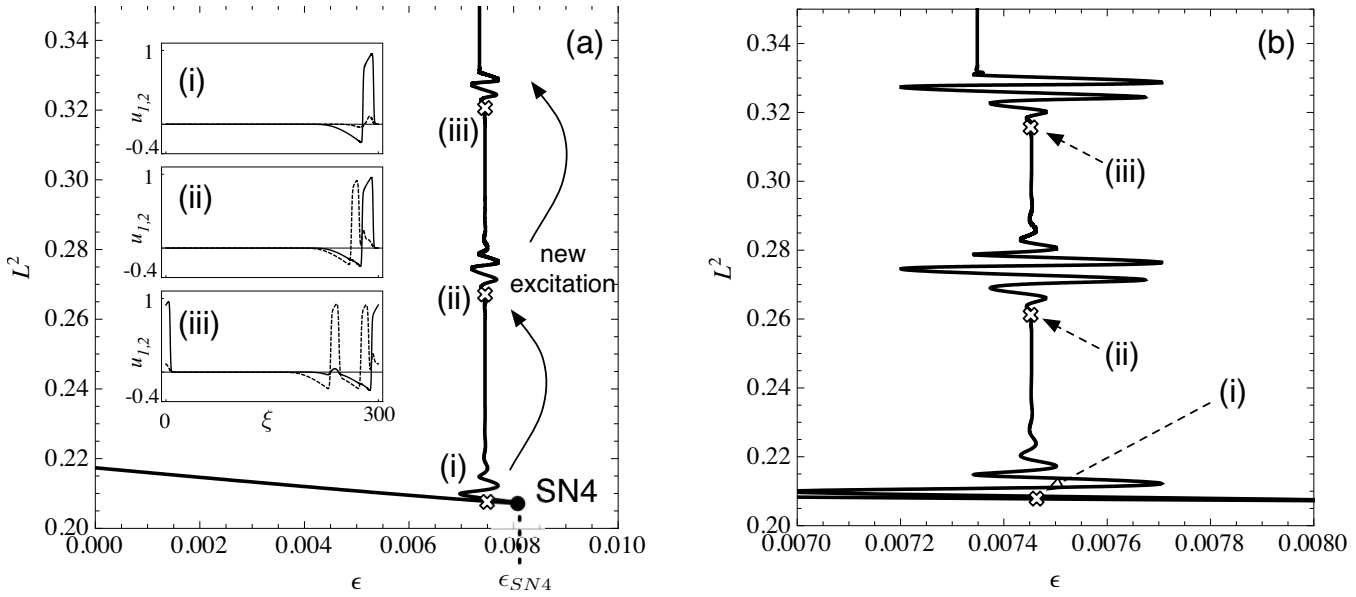

FIG. 7. (a) Bifurcation diagram of a solitary pulse propagating in fiber 2. The stable solution of the solitary pulse disappears at $\epsilon=\epsilon_{\mathrm{SN4}}\simeq 0.008\ 116\ 09$. The solution branch turns back slightly several times, and the L^2 norm increases suddenly in the vicinity of ϵ_{SN4}, which indicates the emergence of a new excitation in fiber 1. Insets: the spatial profile of the solutions labeled (i), (ii), and (iii). The solid lines represent u_2, while the broken lines represent u_1. (b) Magnification of the critical region clearly shows a sudden increase in L^2 norm with successive turning points.

gating speeds. In order to detect whether the synchronization is stable or not, we use the following numerical procedure: we measure the velocities c_1 and c_2 of two pulses propagating in fibers 1 and 2, respectively. The result of $c_1=c_2$ for any $\Delta\kappa$ indicates that the two propagating pulses remain synchronized, although their velocities decrease with an increase in $\Delta\kappa$. In contrast, on decreasing ϵ gradually, we observe a sudden dip in c_2 at a critical difference $\Delta\kappa_c$, whereas c_1 does not change significantly. This result indicates that the synchronization can no longer be sustained for $\Delta\kappa$ beyond the threshold value $\Delta\kappa_c$. Indeed, even if synchronized pulses are initially prepared, they become desynchronized and propagate with different velocities. More precisely, after the synchronized pulses are desynchronized, the propagation speeds are no longer constant, and they oscillate quasi-periodically in time because periodic boundary conditions are imposed. The dependence of the critical difference $\Delta\kappa_c$ on ϵ is shown by the filled circles in Fig. 10 below.

For a more precise observation, we compute the bifurcation diagram of synchronized pulses as a function of $\Delta\kappa$ for $\epsilon=0.007\ 033$ and 0.0071 in Fig. 8(a). The broken line in Fig. 8(a) shows the solution branch of synchronized pulses for $\epsilon=0.0071$. When the coupling strength is sufficiently large, the synchronized pulses are stable for any amount of parameter mismatch, i.e., they are stable for $0\leqslant\Delta\kappa\leqslant 0.25$. When the coupling strength is small, the synchronized solution disappears at a certain value of $\Delta\kappa$ through a SN bifurcation. Let us explain the change in the synchronized pulses along the solution branch [see the thick line in Fig. 8(a)]. The pulses on the upper solution branch near $\Delta\kappa=0$ are almost completely synchronized. The delay between them gradually increases with $\Delta\kappa$ [see pulse profiles (i) in Fig. 8(b)]. When $\Delta\kappa$ increases further, the stable synchronized state suddenly disappears through a SN bifurcation at $\Delta\kappa=\Delta\kappa_{\mathrm{SN1}}\simeq 0.144\ 642$. It is clearly observed in the bifurcation diagram that the solution branch turns back and that the synchronized solution does not exist for $\Delta\kappa>\Delta\kappa_{\mathrm{SN1}}$ for a small coupling strength $\epsilon=0.007033$. This limiting point corresponds to the SN1 bifurcation point in Fig. 5, where the stable synchronized solution meets the unstable phase-locked solution. The critical value $\Delta\kappa_{\mathrm{SN1}}$ depends on the interfiber coupling strength ϵ, and it increases gradually with ϵ. However, the SN1 bifurcation point does not exist for larger values of $\epsilon>\epsilon^*\simeq 0.007\ 033\ 678$. This implies that beyond the critical coupling strength ϵ^*, synchronized pulses become stable for any $0\leqslant\kappa_2\leqslant 0.25$, while there is a phase delay.

The local stability properties of the periodic solutions are described by Floquet theory [58,62]. In order to verify whether or not there are any bifurcations associated with the continuous spectrum, spatial discrete approximation is employed for synchronized pulses.

The time-dependent variation of the local perturbations of the limit cycle after the evolution of each period along the orbit is governed by the monodromy matrix, which can be obtained as a by-product from the solution of the variational equations after each successful convergence of a continuation step. The eigenvalues of the monodromy matrix are the Floquet multipliers and describe the growth or decay of perturbations of our limit cycle (the synchronized pulses). It should be note that for a spatial domain discretized into n grid points, the integration of the variational equations requires solving a system of $8n(8n+1)$ coupled ODEs, which for the problem discussed here is typically the order of 160 000.

For a given set of parameters, the condition $|\lambda|=1$ designates the bifurcation points where the synchronized pulses change stability. For limit-cycle solutions of systems of autonomous ODEs, one multiplier will always satisfy $\lambda=1$ due

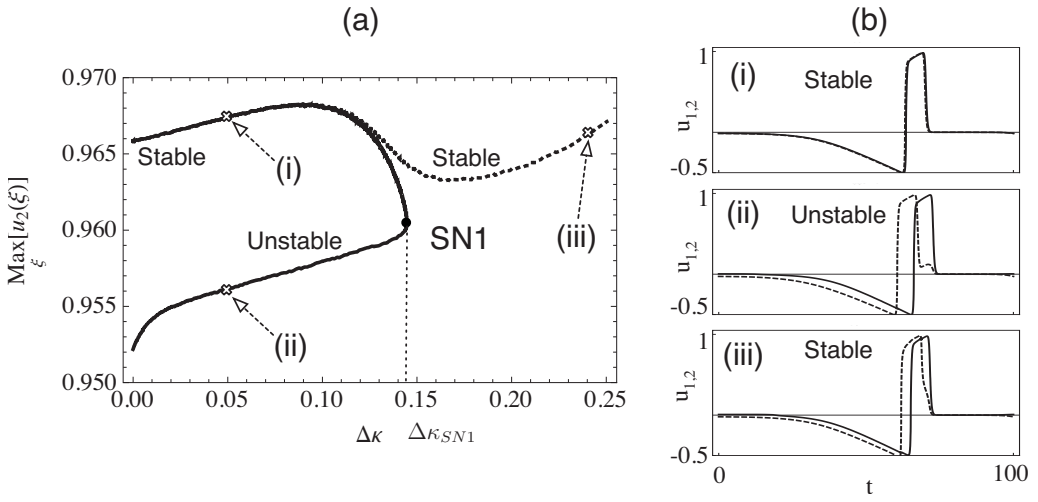

FIG. 8. Bifurcation diagram for the synchronized pulses, with the thick and dotted lines representing ϵ=0.007 033 and 0.0071, respectively. SN1 denotes the saddle-node bifurcation (the collision of stable synchronized pulses and unstable phase-locked pulses solutions), which is the same SN bifurcation labeled SN1 in Fig. 5. $\Delta\kappa_{\mathrm{SN1}}$ is 0.1446 42 for ϵ=0.007 033. The critical value of $\Delta\kappa$ increases gradually with ϵ. The SN1 bifurcation point disappears at $\epsilon^* \simeq 0.007\,033\,75$. The lower branches correspond to unstable phase-locked solutions, while the upper branches correspond to stable solutions with a very small phase delay. (i)–(iii) in (b) show the images of the stable and unstable solutions at the open crosses on the branch shown in (a).

to the time translational invariance of the periodic orbit.

Figure 9 shows that typical spectra of the stable and unstable synchronized solutions for ϵ=0.015. The details of the spectrum transformation are as follows. Initially, the spectrum of stable synchronized pulses contains six isolated discrete complex conjugate eigenvalues, which does not affect the stability of the synchronized pulses, as observed in the bifurcation diagram. On decreasing $\Delta\epsilon$, we observe that stable synchronized pulses are destabilized via SN bifurcation, which corresponds to the bifurcation indicated by SN1 in Fig. 8. In the course of the SN1 bifurcation, the value of an isolated real multiplier increases gradually, and the associated Poincaré map has a Floquet multiplier 1 at the bifurcation point [see Fig. 9(b)]. Finally, the multiplier crosses the unit circle, that is, the synchronized pulses are destabilized through the SN bifurcations.

On $(\epsilon, \Delta\kappa)$ plane, we trace the SN1 (SN2) bifurcation point, which corresponds to the merging of the stable solitary pulse and the unstable phase-locked pulses (the merging of unstable phase-locked pulses and stable synchronized pulses). The solid line (dashed line) in Fig. 10 is the bifurcation curve corresponding to SN1 (SN2) in Fig. 5. It can be seen that a pair of SN bifurcation curves emerges through a codimension-2 cusp singularity. When the coupling strength ϵ increases beyond the value where the cusp singularity occurs, the synchronized pulses are stable for all $0 \leqslant \Delta\kappa \leqslant 0.25$. Although SN1 and SN2 bifurcations do not exist beyond $\Delta\kappa^* \simeq 0.147786$ because they disappear via the codimension-2 cusp singularity, SN3 bifurcation exists for all $\Delta\kappa$, as shown by the thin broken line in Fig. 10. These results are consistent with those obtained in direct numerical simulations.

We also trace the SN4 bifurcation point on the $(\epsilon, \Delta\kappa)$ plane. The dot-dashed line in Fig. 10 shows the SN4 bifurcation curve, where a stable solitary pulse in fiber 2 disappears via an SN bifurcation. When we increase ϵ across the SN4 bifurcation curve, the solitary pulse propagating in fiber 2 is destabilized and a reentrant wave is formed in numerical simulations. The dotted region in Fig. 10 shows the parameter region where a stable reentrant wave is observed. Al-

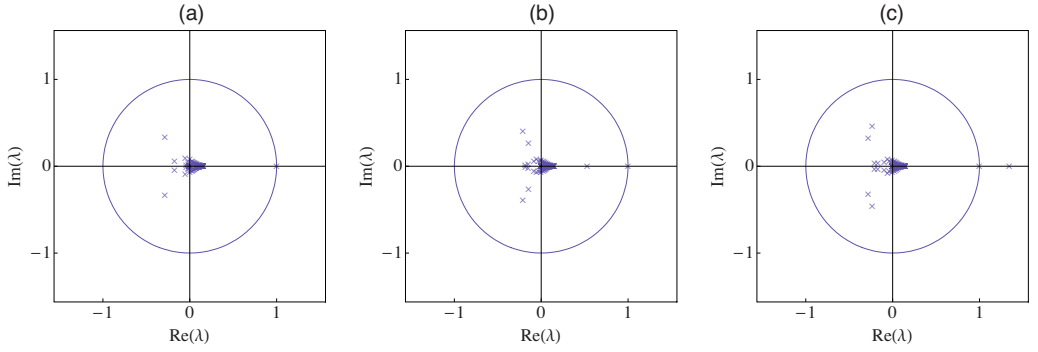

FIG. 9. (Color online) Floquet multipliers for the synchronized pulses with ϵ=0.015. The pictures show the typical change in the spectrum along the solution branch. (a) $\Delta\kappa$=0.05, stable synchronized pulses; (b) $\Delta\kappa$=0.14, stable synchronized pulses in the vicinity of the SN bifurcation; and (c) $\Delta\kappa$=0.144 552, unstable synchronized pulses.

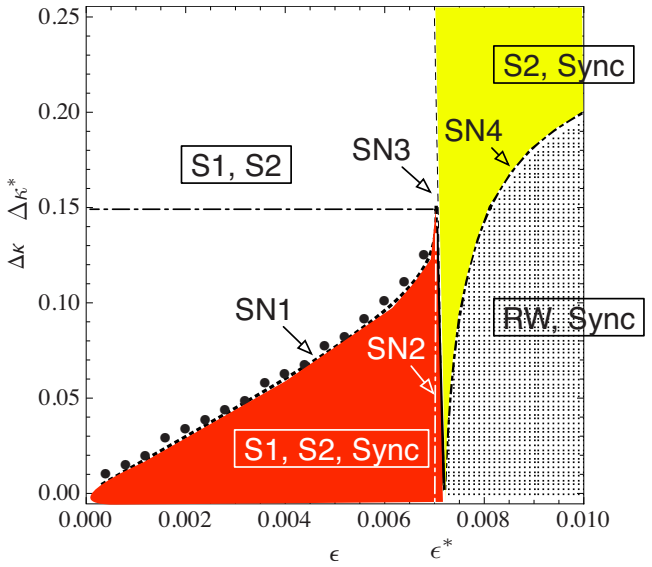

FIG. 10. (Color online) SN bifurcation curves are plotted on $(\epsilon, \Delta\kappa)$. The thick solid line represents the SN2 bifurcation curve corresponding to the merging of the stable solitary pulse and the unstable phase-locked pulses (SN2 in Fig. 5). The thick broken line shows the SN1 curve corresponding to the merging of the unstable phase-locked pulses and stable synchronized pulses (SN1 in Fig. 5). These curves emerge through a codimension-2 cusp singularity $(\epsilon^*, \Delta\kappa^*) = (0.007\,033\,678, 0.147\,786)$ involving a pair of two SN bifurcation curves. The circles show numerically obtained critical differences between intradiffusion coefficients $\Delta\kappa$. The thin broken line shows the SN3 curve (see Fig. 6). The dot-dashed line represents the SN4 curve, at which the solitary pulse in fiber 2 disappears. The parameter space is divided into the following four regions by the existence of solution types: (S1, S2) solitary pulses in fiber 1 (S1) and in fiber 2 (S2) exist; (S1, S2, Sync) S1, S2, and synchronized pulses (Sync) exist; (S2, Sync) S2 and Sync solutions exist; (RW, Sync) reentrant wave (RW) and synchronized-pulse solutions exist. The reentrant waves are numerically stable in the dotted region.

though the dotted area and the SN4 curve represent different bifurcation structures, i.e., the former corresponds to a reentrant wave and the later corresponds to a solitary pulse in fiber 2, the two curves are indistinguishable. This agreement of these bifurcation structures comes from the necessary conditions that a reentrant wave is stable, i.e., both solitary pulses propagating in fibers 1 and 2 are unstable and synchronized pulses are stable. In Fig. 7, we see that successive generations of new supraexcitations are observed along the solution branch beyond the SN4 point. This cascade of new excitations might be related to a reentrant-wave solution. However, because a reentrant wave is not a periodic solution of the traveling wave ODEs, further study of the direct bifurcation analysis of a reentrant wave is required to reveal the relation.

In the reentrant-wave phase, pulses are generated with a characteristic period T_{RW}. The characteristic period of a reentrant wave is calculated as a function of ϵ, and it is found to follow a power law with an exponent of $1/2$, i.e., $T_{\mathrm{RW}} \sim |\epsilon - \epsilon_{\mathrm{SN2}}|^{-1/2}$ near the transition point ϵ_{SN2}. This result implies that SN bifurcation is the onset mechanism of the reentrant wave. On the other hand, stable synchronized pulses are desynchronize across the SN1 and SN3 bifurcation curves on decreasing ϵ gradually. In numerical simulations, these desynchronized pulses propagate with different speeds, and the distance between them increases. However, because periodic boundary conditions are employed, these desynchronized pulses finally form phase-locked pulses. This type of phase-locked pulse was not investigated in this study.

V. SUMMARY

We have investigated the dynamics and bifurcation structures in mutually coupled excitable fibers. Solitary, synchronized, and reentrant waves have been analyzed.

With an increase in the coupling strength ϵ, a solitary pulse propagating in fiber 1 becomes unstable through a SN bifurcation (SN2). At the SN2 bifurcation point, the solution branch turns back, and a new excitation in fiber 2 is suddenly formed. This type of bifurcation is similar to a "canard solution," i.e., a steep increase in the amplitude of oscillation in relaxation systems. However, in this case, the bifurcation is not the Hopf type, but the SN type [9]. A canard excitation emerges in fiber 2 and becomes phase locked with the original solitary pulse in fiber 1. This phase locked solution is unstable, but it becomes stable via a SN bifurcation (SN1) after several turnback points near the SN3 bifurcation point (see Figs. 5 and 6). At the SN1 point, the branch turns in the positive direction of ϵ. The phase difference between the stable pulse-locked pulses continues to decrease until they become completely synchronized as ϵ increases. In other words, by decreasing the coupling strength between fibers, the phase difference between the pulses gradually increases and the synchronized solution disappears through a SN bifurcation (SN1). Further, when the coupling coefficient between these SN bifurcation points is $\epsilon_{\mathrm{SN1}} < \epsilon < \epsilon_{\mathrm{SN2}}$, hysteresis is observed, i.e., both a solitary pulse and synchronized pulses coexist.

The solution of a solitary pulse propagating in fiber 2 disappears via a SN bifurcation (SN4) when ϵ reaches the critical coupling strength ϵ_{SN4}. The solution branch turns back in the negative direction of ϵ at the SN4 point, and successive SN bifurcations occur. The L^2 norm of the solution suddenly increases with successive SN bifurcations. This sudden increase indicates the generation of supraexcitation in fiber 1. Although this bifurcation structure, i.e., the successive generations of supraexcitation, is obtained by analyzing traveling wave ODEs, the $\Delta\kappa$ dependence of the critical coupling strength, beyond which a reentrant wave appears, is almost identical to the SN4 curve. This agreement comes from the fact that the SN4 curve is the critical curve on which the necessary conditions for the existence of a stable reentrant wave hold, i.e., a reentrant wave can be stable only when the solitary pulses in fiber 1 and fiber 2 are unstable and the synchronized pulses are stable. A bifurcation structure such as a cascade of excitations obtained by the analysis of traveling wave ODEs might be related to a reentrant-wave solution.

Synchronized pulses are also destabilized through a SN bifurcation by increasing the difference between the intrafi-

ber diffusion coefficients when the coupling between the fibers is weak. However, synchronized pulses are stable for $0 \leqslant \kappa_2 \leqslant 0.25$ beyond the critical coupling strength $\epsilon^* \simeq 0.007\,033\,678$. The critical coupling strength originates from the emergence of two SN curves in the $(\epsilon, \Delta\kappa)$ parameter space via a codimension-2 cusp singularity.

These complex bifurcation structures arise from the interaction between fibers with different intradiffusion coefficients, while only a traveling-pulse solution exists in a single excitable fiber. Simple excitable fibers, which have FHN-type reaction kinetics, exhibit a different, varied dynamics via a mutual interaction between pulses in laterally coupled fibers since one fiber acts as "hidden variables" for the other fiber.

ACKNOWLEDGMENTS

This study has been partially supported by Grant-in-Aid No. 17022012 for Scientific Research on Priority Areas: "System Study on Higher-Order Brain Functions" from the Ministry of Education, Culture, Sports, Science and Technology of Japan, and by the Ministry of Education, Science, Sports and Culture, Grant-in-Aid for Scientific Research No. (19540390).

[1] *Synchronization: A Universal Concept in Nonlinear Sciences*, edited by J. Kurths, A. Pikovsky, and M. Rosenblum (Cambridge University Press, Cambridge, U.K., 2001).
[2] S. H. Strogatz, Physica D **143**, 1 (2000).
[3] G. Bub, A. Shrier, and L. Glass, Phys. Rev. Lett. **88**, 058101 (2002).
[4] M. Courtemanche, L. Glass, and J. P. Keener, Phys. Rev. Lett. **70**, 2182 (1993).
[5] T. Nomura and L. Glass, Phys. Rev. E **53**, 6353 (1996).
[6] L. Glass and M. E. Josephson, Phys. Rev. Lett. **75**, 2059 (1995).
[7] A. L. Hodgkin and A. F. Huxley, J. Physiol. (London) **117**, 500 (1952).
[8] I. Segev and W. Rall, Trends Neurosci. **21**, 453 (1998).
[9] E. M. Izhikevich, Int. J. Bifurcation Chaos Appl. Sci. Eng. **10**, 1171 (2000).
[10] F. Siegert and C. Weijer, J. Cell. Sci. **93**, 325 (1989).
[11] E. Pálsson and E. C. Cox, Proc. Natl. Acad. Sci. U.S.A. **93**, 1151 (1996).
[12] J. Christoph, M. Eiswirth, N. Hartmann, R. Imbihl, I. Kevrekidis, and M. Bär, Phys. Rev. Lett. **82**, 1586 (1999).
[13] M. P. Cox, G. Ertl, and R. Imbihl, Phys. Rev. Lett. **54**, 1725 (1985).
[14] H. H. Rotermund, W. Engel, M. Kordesch, and G. Ertl, Nature (London) **343**, 355 (1990).
[15] S. Jakubith, H. H. Rotermund, W. Engel, A. von Oertzen, and G. Ertl, Phys. Rev. Lett. **65**, 3013 (1990).
[16] N. Manz, S. Muller, and O. Steinbock, J. Phys. Chem. A **104**, 5895 (2000).
[17] C. T. Hamik and O. Steinbock, Phys. Rev. E **65**, 046224 (2002).
[18] M. Giudici, C. Green, G. Giacomelli, U. Nespolo, and J. R. Tredicce, Phys. Rev. E **55**, 6414 (1997).
[19] M. C. Eguia and G. B. Mindlin, Phys. Rev. E **60**, 1551 (1999).
[20] J. M. Méndez, J. Aliaga, and G. B. Mindlin, Phys. Rev. E **71**, 026231 (2005).
[21] A. Zaikin and A. M. Zhabotinsky, Nature (London) **225**, 535 (1970).
[22] A. T. Winfree, Science **175**, 634 (1972).
[23] G. Ertl, Science **254**, 1750 (1991).
[24] L. Yang and I. R. Epstein, Phys. Rev. Lett. **90**, 178303 (2003).
[25] M. Hildebrand, J. Cui, E. Mihaliuk, J. Wang, and K. Showalter, Phys. Rev. E **68**, 026205 (2003).
[26] R. Neubecker and B. Gütlich, Phys. Rev. Lett. **92**, 154101 (2004).
[27] J. García-Ojalvo and R. Roy, Phys. Rev. Lett. **86**, 5204 (2001).
[28] H. Agmon-Snir, C. E. Carr, and J. Rinzel, Nature (London) **393**, 268 (1998).
[29] C. Koch and I. Segev, Nat. Neurosci. Suppl. **3**, 1171 (2000).
[30] I. Segev and E. Schneidman, J. Physiol. (Paris) **93**, 263 (1999).
[31] I. Segev and M. London, Science **290**, 744 (2000).
[32] T. Yanagita, Phys. Rev. E **76**, 056215 (2007).
[33] A. Arvanitaki, J. Neurophysiol. **5**, 89 (1942).
[34] B. Katz and O. Schmitt, J. Physiol. (London) **97**, 471 (1940).
[35] J. Jefferys, Physiol. Rev. **75**, 689 (1995).
[36] *Clinical Cardiac Electrophysiology: Techniques and Interpretation*, edited by M. E. Josephson, 2nd ed. (Lea & Febiger, Philadelphia, 1993).
[37] *Cardiac Arrhythmias: An Integrated Approach for the Clinician*, edited by E. N. Prystowsky and G. J. Klein, (McGraw-Hill, New York, 1994).
[38] Y. Nagai, H. González, A. Shrier, and L. Glass, Phys. Rev. Lett. **84**, 4248 (2000).
[39] T. Yanagita, Y. Nishiura, and R. Kobayashi, Phys. Rev. E **71**, 036226 (2005).
[40] D. D. Streeter, Jr., H. M. Spotnitz, D. P. Patel, J. Ross, Jr., and E. H. Sonnenblick, Circ. Res. **24**, 339 (1969).
[41] A. T. Winfree, Chaos **8**, 1 (1998).
[42] J. C. Neu and W. Krassowska, Crit. Rev. Biomed. Eng. **21**, 137 (1993).
[43] J. P. Keener, SIAM J. Appl. Math. **49**, 210 (1989).
[44] M. A. Allessie, F. I. M. Bonke, and F. J. G. Schopman, Circ. Res. **33**, 54 (1973).
[45] V. I. Krinsky, Pharmacol. Ther. [B] **3**, 539 (1978).
[46] D. Debanne, Nat. Rev. Neurosci. **5**, 304 (2004).
[47] G. Söhl, S. Maxeiner, and K. Willecke, Nat. Rev. Neurosci. **6**, 191 (2005).
[48] B. Katz and O. H. Schmitt, J. Physiol. (London) **100**, 369 (1942).
[49] J. Kocsis, J. Ruiz, and K. Cummins, Exp. Brain Res. **100**, 151 (1982).
[50] H. Suetani, T. Yanagita, and K. Aihara, Int. J. Bifurcation Chaos Appl. Sci. Eng. **18**, 2289 (2008).
[51] V. N. Biktashev and M. A. Tsyganov, Proc. R. Soc. London, Ser. A **461**, 3711 (2005).

[52] J. H. E. Cartwright, E. Hernández-García, and O. Piro, Phys. Rev. Lett. **79**, 527 (1997).
[53] A. Panfilov and A. Holden, Phys. Lett. A **147**, 463 (1990).
[54] A. Panfilov and B. Basiev, Chaos, Solitons Fractals **1**, 119 (1991).
[55] A. Palmer, J. Brindley, and A. Holden, Bull. Math. Biol. **54**, 1039 (1992).
[56] I. P. Mariño, M. de Castro Rodríguez, V. Pérez-Muñuzuri, M. Gómez-Gesteira, L. O. Chua, and V. Pérez-Villar, IEEE Trans. Circuits Syst., I: Fundam. Theory Appl. **42**, 665 (1995).
[57] M. Cross and P. Hohenberg, Rev. Mod. Phys. **65**, 851 (1993).
[58] R. Seydel, *Practical Bifurcation and Stability Analysis* (Springer, New York, 1994).
[59] E. J. Doedel, R. C. Paffenroth, A. R. Champneys, T. F. Fairgrieve, Y. A. Kuznetsov, B. Sandstede, and X. Wang, Caltech Technical Report, 2001 (unpublished).
[60] T. Yanagita, T. Ichinomiya, and Y. Oyama, Phys. Rev. E **72**, 056218 (2005).
[61] Y. Oyama, T. Yanagita, and T. Ichinomiya, Prog. Theor. Phys. Suppl. **161**, 389 (2006).
[62] *Elementary Stability and Bifurcation Theory*, edited by G. Iooss and D. Joseph, 2nd ed. (Springer, New York, 1997).